Radiological Physics and Technology
https://doi.org/10.1007/s12194-022-00690-2

RESEARCH ARTICLE

Shielding performance of multi-metal nanoparticle composites for diagnostic radiology: an MCNPX and Geant4 study

Nikan Asadpour[1] · Reza Malekzadeh[2] · Saeed Rajabpour[3] · Soheila Refahi[4] · Parinaz Mehnati[2] · Ahmad Shanei[1]

Received: 14 August 2022 / Revised: 27 November 2022 / Accepted: 28 November 2022

Abstract
Lead-free polymer composite shields are used in diagnostic radiology to protect patients from unnecessary radiation exposure. This study aimed to examine and introduce the radiation-shielding properties of single- and multi-metal nanoparticle (NP)-based composites containing Bi, W, and Sn using Geant4, MCNPX, and XCom for radiological applications. The mass attenuation coefficients and effective atomic numbers of single- and multi-metal NP-loaded polymer composites were calculated using the Geant4 and MCNPX simulation codes for X-ray energies of 20–140 keV. The nano-sized fillers inside the polydimethylsiloxane (PDMS:C_2H_6SiO) matrix included W ($K = 69.5$ keV), Bi ($K = 90.5$ keV), and Sn ($K = 29.20$ keV). For single-metal shields, one filler was used, while in multi-metal shields, two fillers were required. The MCNPX and Geant4 simulation results were compared with the XCom results. The multi-metal NP composites exhibited higher attenuation over a larger energy range owing to their attenuation windows. In addition, $Bi_2O_3 + WO_3$ NPs showed a 39% higher attenuation at 100–140 keV, and that of $Bi_2O_3 + SnO_2$ NPs was higher at 40–60 keV. Meanwhile, the $WO_3 + SnO_2$ NPs exhibited lower attenuation. The difference between the results obtained using Geant4 and XCom was less than 2%, because these codes have similar simulation structures. The results show that the shielding performance of the $Bi_2O_3 + WO_3$ filler is better than that of the other single- and multi-metal fillers. In addition, it was found that the Geant4 code was more accurate for simulating radiation composites.

Keywords Radiation protection · Polymer composite · Nanoparticle · Monte Carlo

1 Introduction

Ionizing radiation is used for imaging patients, and more than ten million diagnostic radiology procedures have been conducted worldwide [1]. Accordingly, it is necessary to modulate radiation damage and reduce the absorbed dose, particularly for radiosensitive organs, such as the lens of the eye, thyroid, and breast. Previous studies have demonstrated that radioprotective shields can be used to optimize radiation, except in automatic exposure control systems [2–6]. Common materials that protect against radiation include high-density rigid materials, such as Pb. However, such materials have some disadvantages including extreme toxicity, heavy weight, and low mechanical and chemical stabilities [7, 8]. Thus, researchers have recently proposed new types of radiation protectors for low-energy photons [6].

Polymer composites containing high-atomic-number metal fillers in the form of microparticles and nanoparticles (NPs) have been widely investigated as alternative radiation-shielding materials because of their flexibility, structural conformability, nontoxicity, light weight, and low cost [5, 6, 9, 10].

Numerical modeling is one of the most accurate methods used to determine and optimize the properties of radiation-shielding materials. Computer simulation codes based on

✉ Parinaz Mehnati
parinazmehnati8@gmail.com

✉ Ahmad Shanei
shanei@med.mui.ac.ir

1 Medical Physics Department, Faculty of Medicine, Isfahan University of Medical Sciences, Isfahan, Iran

2 Medical Physics Department, Faculty of Medicine, Tabriz University of Medical Sciences, Tabriz, Iran

3 Medical Physics Department, Faculty of Medicine, Urmia University of Medical Sciences, Urmia, Iran

4 Medical Physics Department, Faculty of Medicine, Ardabil University of Medical Sciences, Ardabil, Iran

Published online: 23 December 2022

mathematical methods are widely used for this purpose. Notably, Monte Carlo (MC) codes (including Geant4 and MCNPX) are extremely useful for assessing the doses absorbed by organs, thereby providing information that cannot be clinically assessed. MC codes are used to simulate physical interactions via three-dimensional simulation geometries [11].

Mendes et al. used Geant4 and MCNPX to determine the dose reduction for radiosensitive organs using Bi composite shields. They reported that the relative difference between the simulations and measurements was less than 10% [12].

The use of fillers in a polymer matrix at the nanoscale can significantly enhance the polymer's physical properties, such as thermal stability, electrical insulation, and mechanical strength [10, 13]. In addition, the polymer can efficiently attenuate radiation because NPs are uniformly dispersed in the matrix with low agglomeration, which enhances the radiation-shielding ability of the material [14]. A study conducted on the effect of the size of Bi_2O_3 particles dispersed in Si on X-ray transmission has reported that this effect is stronger at lower photon energies [15, 16]. Malekzadeh et al. investigated $BaSO_4$, WO_3, and PbO microparticles, as well as NPs with Si–resin-based composites. They reported that shields fabricated from NPs had higher mass attenuation coefficients (up to 17%) than those fabricated from microparticles. The mass attenuation coefficient and effective atomic number are known to be important parameters for explaining photon attenuation by materials constituting multiple elements, such as polymer composite shields [17].

Based on literature reviews, researchers have investigated the effectiveness of composite shields in the presence of single NPs for different types of metals (K-edges) [5, 6]. It has been established that heavy metal NPs show acceptable radiation-protection properties owing to their high atomic number and absorption edge. Studies regarding the effect of the simultaneous use of two NPs with different atomic numbers, absorption K-edges, and concentrations are inadequate. Thus, the current study was designed to address this research gap. In particular, to lock the photon energy window, the effectiveness of polymer composite shields with two metal NPs was investigated. This aspect has not been fully investigated previously.

A multi-metal polymer composite (MMPC) with a high-atomic-number filler (NPs with different K-edges to close the energy window), instead of using a single-metal polymer composite (SMPC), may provide higher radiation protection over the wide range of photon energies used in diagnostic radiology (40–140 keV) [6]. Therefore, in this study, we investigated whether MMPCs fabricated with Bi (for high-energy photons), W (for middle-energy photons), and Sn (for low-energy photons) with different concentrations and K-edges were more effective than SMPCs. The mass attenuation coefficients and effective atomic numbers of single- and multi-metal polymer composites were comprehensively calculated using MC codes (MCNPX and Geant4), and their shielding properties were compared. Finally, the most effective composition was introduced as a novel MMPC for radiation-shielding purposes in diagnostic radiology.

2 Methods and materials

2.1 Theoretical background

When a mono-energetic beam interacts with matter, the intensity of the beam is attenuated according to the Beer–Lambert law, given by [18]:

$$I(x) = I_0 e^{-\mu x} \tag{1}$$

where I_0 and I represent the incident and attenuated photon intensities, respectively, x is the shield thickness (cm), and μ is the linear attenuation coefficient (1/cm).

The mass attenuation coefficient (μ/ρ) was employed to eliminate the dependence of μ on the material density ρ. In addition, μ_m is a measure of the probability of interactions between photons and matter [19], and is given for any chemical compound or a mixture of elements by the following:

$$\mu_m = \sum_i w_i \left(\frac{\mu}{\rho}\right)_i \tag{2}$$

where w_i and $(\mu/\rho)_i$ represent the fractional weight and total μ_m of the ith constituent in a mixture, respectively. These were obtained using XCom software [20].

The effective atomic number Z_{eff} describes the properties of composite materials (compounds or mixtures) in terms of equivalent elements that vary with energy. The values of μ_m were used to calculate Z_{eff} according to [21]:

$$Z_{eff} = \frac{\sum_i f_i A_i (\mu_m)_i}{\sum_i f_i \frac{A_i}{Z_i} (\mu_m)_i} \tag{3}$$

where f_i is the molar fraction of the mixture/compound ($\Sigma f_i = 1$), A_i is the atomic mass, and Z_i is the atomic number of the ith constituent.

In this study, the MCNPX6 and Geant4 codes and the XCom database were used to model the radiation transport and interaction of photons with a material. The difference between the μ_m values obtained using MCNPX, Geant4, and XCom was determined using:

$$\text{Diff}(\%) = \left|\frac{\mu_1 - \mu_2}{\mu_1}\right| \times 100. \tag{4}$$

The nano-sized fillers inside the polydimethylsiloxane (PDMS:C_2H_6SiO) matrix included Pb (K = 88.00 keV), W

($K = 69.5$ keV), Bi ($K = 90.5$ keV), and Sn ($K = 29.20$ keV). The NPs in each model were considered spheres with the diameter of 100 nm.

In this study, two different methods of using NPs were evaluated in the construction of polymer composite shields. First, one of the metal NPs was used as a filler, and in the second method, two NPs were used in the form of a binary combination.

SMPCs comprise two filling elements (reinforcement) on a polymer base (matrix). These shields were simulated in the PDMS matrix with three fillers, bismuth oxide, tin oxide, and tungsten oxide, with mass ratios of 10%, 20%, and 40%, respectively. Regarding the MMPCs, the binary combination of fillers with the same three mass ratios was simulated. In this manner, Bi–Sn, Bi–W, and W–Sn shields were combined with a PDMS matrix with equal shares and mass ratios of 10%, 20%, and 40%.

2.2 MCNPX code

The MCNPX code (version 2.6.0, Los Alamos National Laboratory cross-sectional library data) was employed in this study.

The input parameters for MCNPX, including cell card, surface card, material card, and features of the energy sources, were defined in the input files. The entire set of simulation geometries was inserted into a cylindrical space with the height of 100 cm and diameter of 30 cm (Fig. 1). Thereafter, a surface source with the diameter of 5 mm was defined in the MCNPX data card using PAR, POS, ERG, RAD, AXS, VEC, and DIR commands [15]. Lattice (LAT) and universe (U) cards were used to define the matrix and fillers, and mono-energetic beams with energies of 20–140 keV were simulated to determine μ_m for all study samples. Mono-energetic beams were selected from the X-ray machines found in diagnostic radiology laboratories based on their availability for further experimental studies [22].

All calculations were performed only in the photon transportation mode to reduce errors. The F4 tally, which scored the flux (n/cm^3) of photons entering the detector volume, was used to determine the photon fluence entering the detector cell. Subsequently, the simulations were performed for 3 min on a personal computer (ASUS N56VM laptop with Intel® Core™ i5-3210 M CPU @ 2.50 GHz and 6.00 GB of RAM). Figure 1a depicts the narrow-beam geometry of the advanced MCNPX code, including the source, collimators, and detector.

The composition of all shielding samples, weight fraction of each element, and MCNPX ID of elements is detailed in Table 1.

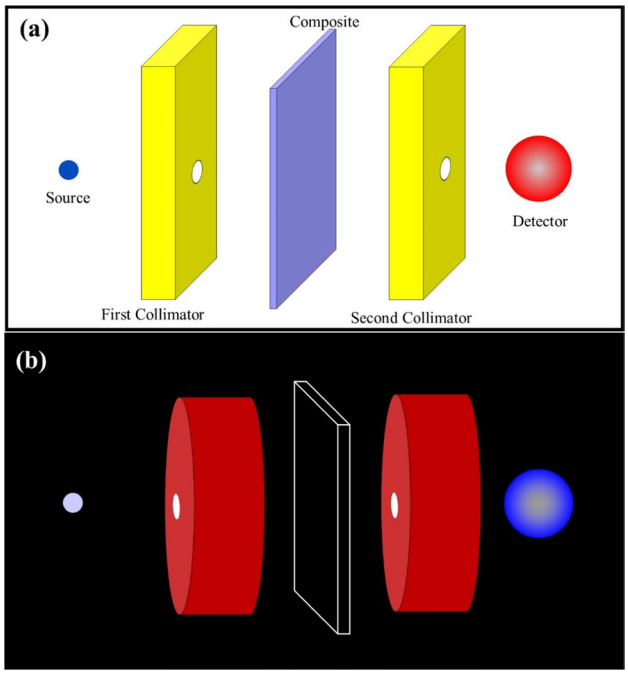

Fig. 1 Actual simulation geometries created using visual editor for **a** MCNPX and **b** Geant4

2.3 Geant4 toolkit

Geant4 (v10.07 p02) was used as an open-source MC toolkit for three-dimensional particle radiation transport modeling [23].

The G4EmLivermorePhysics constructor with the secondary particle production threshold of 0.1 mm was employed for the composites' radiation-shielding applications. A Geant4 advanced narrow-beam geometry was simulated, as shown in Fig. 1b. Shielding materials were defined based on the weight fractions of the composites and their densities. They were then tested as shielding samples at energies in the range of 20–140 keV. Simulations were performed for 10 million incident photons to provide an acceptable statistical uncertainty of $< 1\%$.

2.4 XCom standard database

NIST XCom (Photon Cross Sections Database, National Institute of Standards and Technology, Maryland, USA) was used to obtain the attenuation coefficients [24, 25]. This database can provide partial cross sections, total cross sections, and attenuation coefficients for different interaction processes, such as coherent and incoherent scattering, pair production, and photoelectric absorption, for different elements, compounds, and mixtures, at energies of 1–100 GeV.

XCom data are used in most shielding studies as a criterion for evaluating the accuracy and precision of the

Table 1 Elemental composition of samples simulated using MCNPX Monte Carlo (MC) code

Composite		Density (g/cm^3)	Element	Weight fraction (%)	MCNPX ID
Filler	Matrix (PDMS)				
0.05 wt% Bi_2O_3 0.05 wt% WO_3	0.90 wt%	1.236	H	0.07340	1001.60c
			C	0.29155	6012.60c
			O	0.20968	8016.60c
			Si	0.34087	14,028.60c
			W	0.03965	74,184.60c
			Bi	0.04485	83,209.60c
0.05 wt% Bi_2O_3 0.05 wt% SnO_2		1.236	H	0.07340	1001.60c
			C	0.29155	6012.60c
			O	0.20995	8016.60c
			Si	0.34087	14,028.60c
			Sn	0.03938	50,119.60c
			Bi	0.04485	83,209.60c
0.05 wt% WO_3 0.05 wt% SnO_2		1.234	H	0.07340	1001.60c
			C	0.29155	6012.60c
			O	0.21515	8016.60c
			Si	0.34087	14,028.60c
			Sn	0.03938	50,119.60c
			W	0.03965	74,184.60c
0.10 wt% Bi_2O_3 0.10 wt% WO_3	0.80 wt%	1.364	H	0.06524	1001.60c
			C	0.25916	6012.60c
			O	0.20361	8016.60c
			Si	0.30299	14,028.60c
			W	0.07930	74,184.60c
			Bi	0.08970	83,209.60c
0.10 wt% Bi_2O_3 0.10 wt% SnO_2		1.363	H	0.06524	1001.60c
			C	0.25916	6012.60c
			O	0.20414	8016.60c
			Si	0.30299	14,028.60c
			Sn	0.07877	50,119.60c
			Bi	0.08970	83,209.60c
0.10 wt% WO_3 0.10 wt% SnO_2		1.358	H	0.06524	1001.60c
			C	0.25916	6012.60c
			O	0.21454	8016.60c
			Si	0.30299	14,028.60c
			Sn	0.07877	50,119.60c
			W	0.07930	74,184.60c
0.20 wt% Bi_2O_3 0.20 wt% WO_3	0.60 wt%	1.720	H	0.04893	1001.60c
			C	0.19437	6012.60c
			O	0.19146	8016.60c
			Si	0.22725	14,028.60c
			W	0.15860	74,184.60c
			Bi	0.17940	83,209.60c
0.20 wt% Bi_2O_3 0.20 wt% SnO_2		1.717	H	0.04893	1001.60c
			C	0.19437	6012.60c
			O	0.19252	8016.60c
			Si	0.22725	14,028.60c
			Sn	0.15757	50,119.60c
			Bi	0.17940	83,209.60c

Table 1 (continued)

Composite		Density (g/cm^3)	Element	Weight fraction (%)	MCNPX ID
Filler	Matrix (PDMS)				
0.20 wt% WO_3 0.20 wt% SnO_2		1.701	H	0.04893	1001.60c
			C	0.19437	6012.60c
			O	0.21332	8016.60c
			Si	0.22725	14,028.60c
			Sn	0.15754	50,119.60c
			W	0.15860	74,184.60c

PDMS polydimethylsiloxane

advanced model. Also, in the Xcom, NPs are assumed in the molecular structure of the composite, which is the best and most ideal form of the composition. For this reason, in terms of structure, it is considered as a reference in the design of composite shields [25]. The MCNPX and Geant4 simulation results were compared by calculating the theoretical values of μ_m for different MMPCs and SMPCs using XCom.

2.5 Verification and validation of advanced models

The accuracy and credibility of the MC models were assessed by comparing the MC results with data provided by XCom for a conventional Pb shield [26]. The linear attenuation coefficients of Pb were calculated and compared with standard XCom data [22]. Finally, the validated input codes were used to calculate the radiation mass attenuation coefficients of the samples.

3 Results

3.1 Validation of the simulation geometry

At first, the simulated narrow-beam geometry was validated as follows: The linear attenuation coefficients of Pb (density = 11.35 g/cm^3) were calculated at photon energies of 20–140 keV using MCNPX and Geant4 and then compared with the XCom results. A maximum difference of 1% was observed between the results. After ensuring the accuracy of the advanced MCNPX and Geant4 codes, the composites were simulated in the presence of the metal NPs.

3.2 Performance of single-metal polymer nanocomposite (effect of concentration and K-edge)

Figure 2 presents the values of μ_m for SMPCs at energies between 20 and 140 keV. Bi_2O_3, WO_3, and SnO_2 NPs were used in the MCNPX code at concentrations of 10%, 20%, and 40% in the PDMS polymer matrix.

3.3 Performance of multi-metal polymer nanocomposite

The values of μ_m were calculated for polymer composite shields with 90%, 80%, and 60% PDMS as the composite matrix, as well as 10%, 20%, and 40% NPs as fillers at energies of 20, 40, 60, 80, 100, 120, and 140 keV. The values of μ_m obtained using MCNPX, Geant4, and XCom are shown in Figs. 3, 4, and 5, respectively.

3.4 Comparison of MCNPX, Geant4, and XCom results

The differences between the results obtained using MCNPX, Geant4, and XCom are listed in Tables 2, 3, and 4, respectively.

3.5 Effect of Z_{eff} on nanocomposite radiation attenuation

The variation in Z_{eff} with the photon energy for the nine shields is depicted in Fig. 6. The value of μ_m as well as atomic weights of each element used in the formula for Z_{eff} was obtained from the XCom program data.

4 Discussion

As shown in Fig. 2a, the attenuation coefficient increased with the concentration of NPs. This is consistent with the findings of El-Khatib et al., who reported that μ_m significantly increased with the concentration of micro-cadmium oxide (CdO) and nano-CdO in composites at photon energies of 59.53–121.78 keV [27]. In addition, Mehnati et al. showed that when the concentration of Bi_2O_3 NPs in a

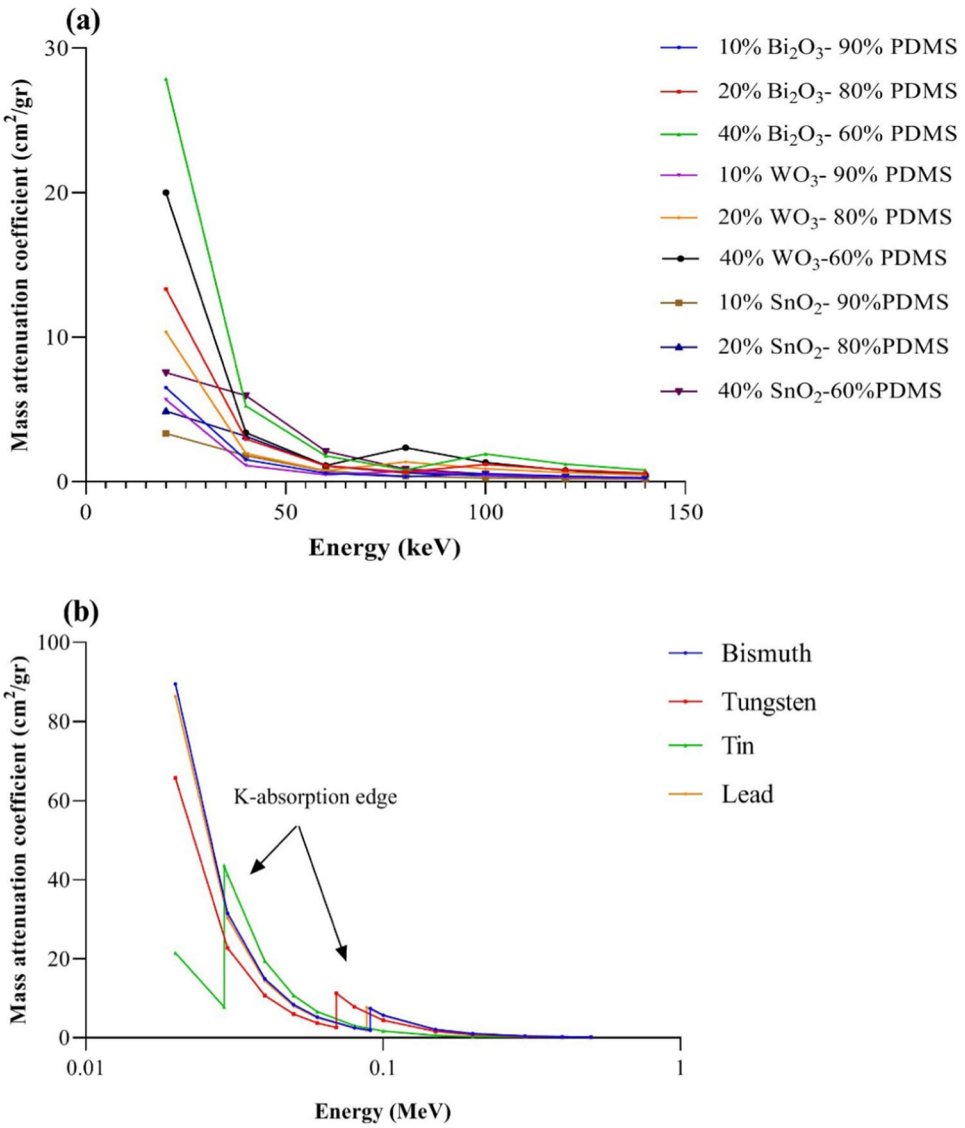

Fig. 2 **a** Comparison of mass attenuation coefficients for single-metal nanocomposites of Bi_2O_3, WO_3, SnO_2 at three different concentrations and energies of 20–140 keV. **b** Mass attenuation coefficients of investigated elements (plot data obtained from XCom database). *PDMS* polydimethylsiloxane

polymer composite increased by 10%, the radiation-protection efficiency increased by approximately 9% [28].

The mass attenuation coefficients for the pure NPs obtained from the XCom standard data are compared in Fig. 2b. As is evident in Fig. 2, when the weight of bismuth oxide in the Bi–Si SMPC increased from 20 to 40 wt% at 60 keV, the μ_m value increased by 60% (from 1.1138 to 1.7793 $cm^2\ g^{-1}$). In addition, from Fig. 4, the μ_m value in the Bi-W MMPC was 39.82% higher than that of the W-Sn MMPC at 100 keV (from 1.615 to 0.972 $cm^2\ g^{-1}$). El-Khatib et al. also found that a 46% increase in 59.53 keV occurs when the weight of nano-CdO increased from 40 to 60 wt% (from 1.3748 to 2.5620 $cm^2\ g^{-1}$) [27].

As the energy increased, the mass attenuation coefficients of all the samples decreased. Close to the K-edge, the photon energy is completely absorbed by the electrons, and the probability of the photoelectric effect significantly increases, which improves the shielding performance [28]. The results show that the two K-edges provided higher attenuation, and this advantage was applied by creating a new MMPC shield with two fillers selected among Bi, W, and Sn NPs.

In the intermediate-energy range, there was a discontinuity in the attenuation coefficients of the shields containing Bi_2O_3 and WO_3, which was because of the K-edge of Bi and W. The K-edge of Bi_2O_3 is 90.5 keV. As shown in Figs. 3, 4, and 5, the μ_m values at 100 keV increased in the Bi–W and Bi–Sn nanocomposite shields, in contrast to the general declining trend. The value of μ_m at this energy was larger than those at 80 and 120 keV.

This abrupt increase was observed for the WO_3 shields at 80 keV because its K-edge was 69.5 keV. Unlike in the Bi_2O_3 and WO_3 shields, this discontinuity was not observed in the SnO2 nanocomposite shields. This could be because the absorption edge (29.20 keV) was between 20 and

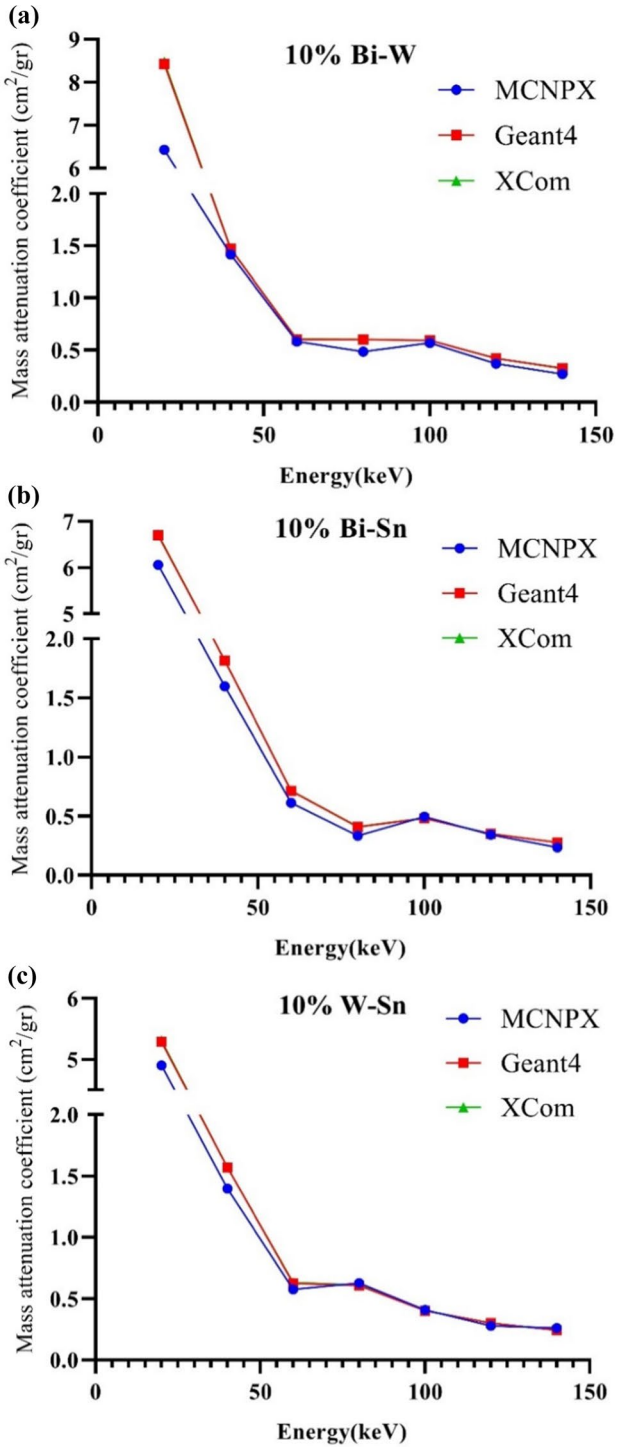

Fig. 3 Mass attenuation coefficients obtained using MCNPX, Geant4, and XCom at energies of 20–140 keV for **a** Bi_2O_3 and WO_3 shield, with 10% nanoparticles (NPs), **b** Bi_2O_3 and SnO_2 shield, with 10% NPs, and **c** WO_3 and SnO_2 shield, with 10% NPs

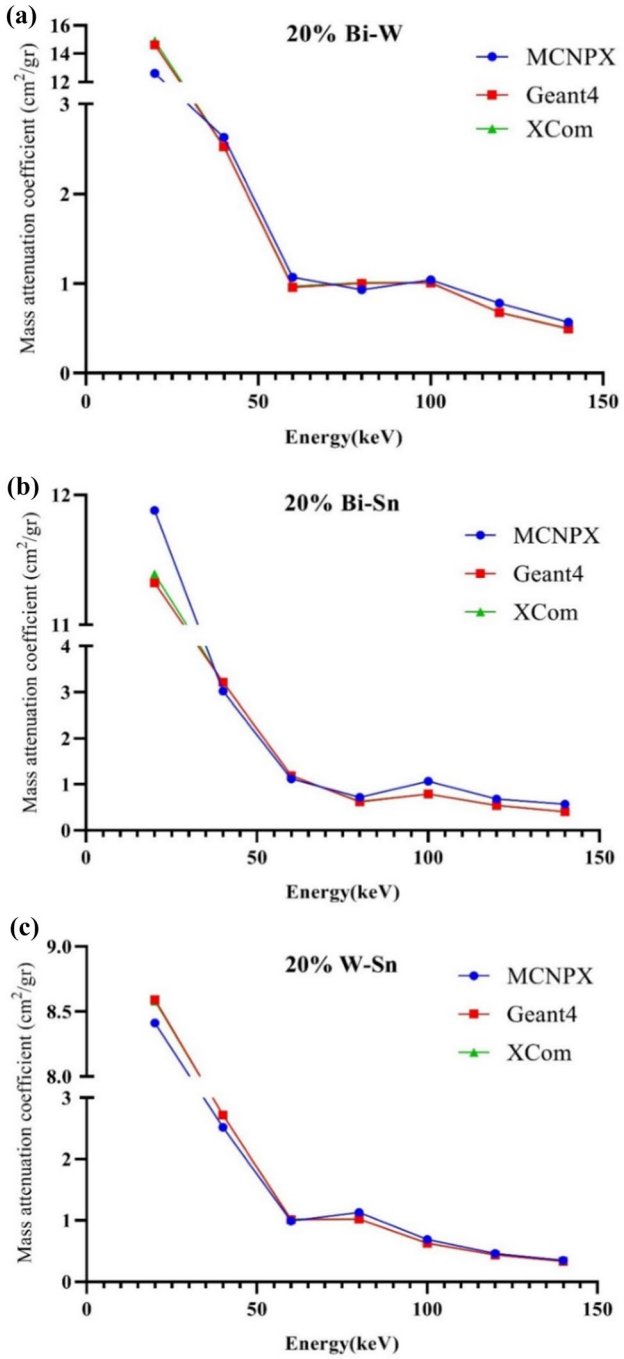

Fig. 4 Mass attenuation coefficients obtained using MCNPX, Geant4, and XCom at energies of 20–140 keV for **a** Bi_2O_3 and WO_3 shield, with 20% NPs, **b** Bi_2O_3 and SnO_2 shield, with 20% NPs, and **c** WO_3 and SnO_2 shield, with 20% NPs

40 keV, and the mass attenuation coefficient at 20 keV was higher than that obtained at other energies. Therefore, the increase in the attenuation coefficient due to the K-edge at 40 keV was different from that of the other two fillers at energies greater than 20 and 60 keV. The attenuation coefficient decreased as the energy decreased from 20 to 40 keV. Finally, the shielding performance of the Bi–W fillers was better than that of the other multi-metal nanocomposites at all concentrations and energies.

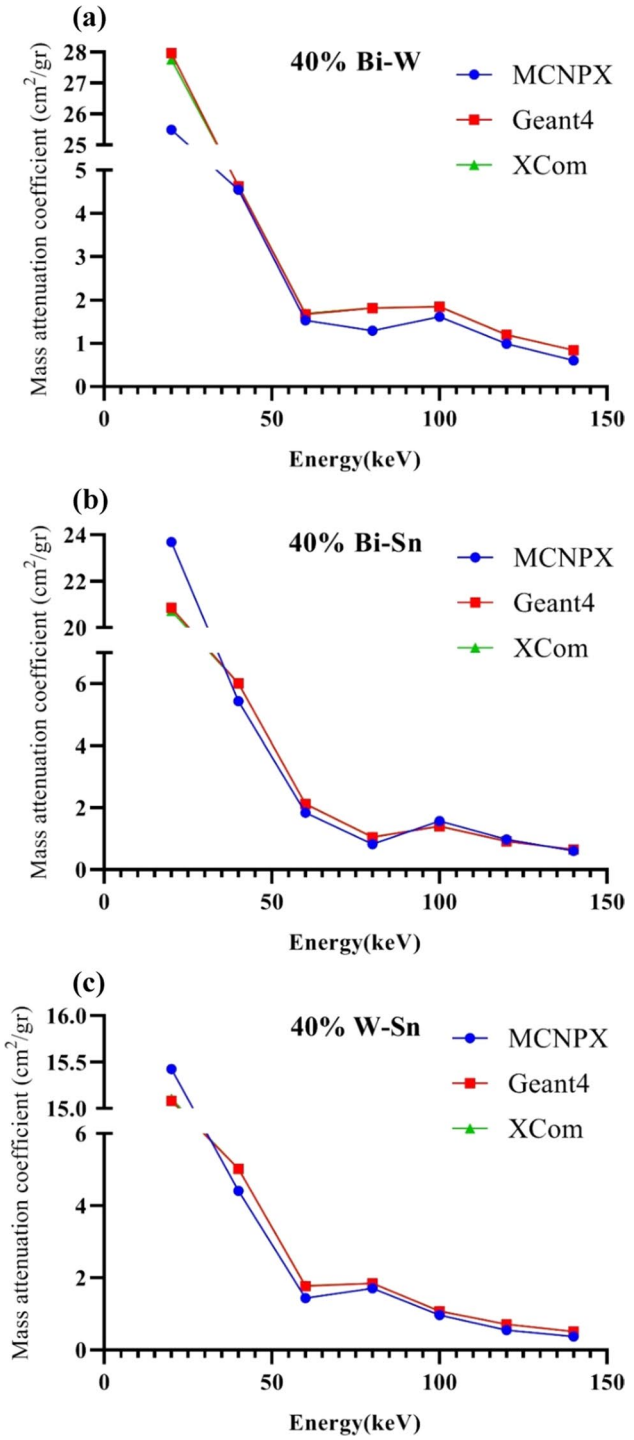

Fig. 5 Mass attenuation coefficients obtained using MCNPX, Geant4, and XCom at energies of 20–140 keV for **a** Bi_2O_3 and WO_3 shield, with 40% NPs, **b** Bi_2O_3 and SnO_2 shield, with 40% NPs, and **c** WO_3 and SnO_2 shield, with 40% NPs

Sayyadi et al. [29] used the MC method to investigate the radiation-shielding properties of silicone rubber-based composites doped with various metal NPs. They reported that all the multi-metal composites exhibited optimal shielding properties and approximately 8% higher attenuation than single-metal composites [29]. This behavior of the mass attenuation coefficient with respect to energy could be because of the photoelectric effect, which was dominant in this energy range (20–140 keV). In particular, below 100 keV, the cross section of the photoelectric interaction was predominant because the photons at this energy were prone to absorption, mainly by the photoelectric effect, depending on $Z^4/E^{3.5}$, where Z is the atomic number of the absorbing element and E is the incident photon energy [30].

The attenuation coefficient at 20 keV was significantly higher than those obtained at other energies, and it rapidly decreased as the energy increased from 20 to 40 keV. Tekin et al. obtained a similar result in another study on concrete blended with WO_3 and Bi_2O_3 microparticles and NPs using MC codes. They found that the decrease in μ_m at lower energies was faster than that at higher energies [9]. Therefore, the μ_m value was increased using a filler with a higher atomic number in the polymer matrix, which had a strong photon absorption capability. However, as the photoelectric cross section was inversely proportional to $E^{3.5}$, μ_m rapidly decreased as the photon energy increased. As the probability of the photoelectric effect increased, more rays were absorbed and the shielding performance improved. El-Khatib et al. conducted a similar study on CdO micro- and nano-fillers with high-density polyethylene and reported similar results [27].

As shown in Tables 2, 3, 4, molecular simulations were performed using Geant4 and XCom, and the results of these two methods were remarkably close (< 2%). This implies that the filler molecules were uniformly dispersed throughout the polymer matrix. As aforementioned, in the MCNPX code, spherical NPs were distributed in the PDMS matrix. This is closer to the actual state than to the theoretical state [31].

This type of simulation caused more differences between the results of MCNPX and other methods. If the standard XCom data were used as a reference, the maximum difference from the Geant4 results was 2.02% for 20 wt% Bi–Sn NPs and 140 keV. The maximum difference obtained from the MCNPX results is 39.02% under the same conditions. Malekzadeh et al. showed that the μ_m values for Bi–Si composites in nano-sized fillers calculated using the MCNPX code were close to the experimental results [22]. Therefore, Geant4 was more accurate in simulating the performance of radiation composites because of the manner in which the NPs were defined in this code. Singh et al. calculated μ_m and Z_{eff} for steel alloys using Geant4 and MCNP at different gamma-ray energies. The results obtained using both codes are in good agreement with the theoretical XCom data. Moreover, they reported that both simulation codes could be used to determine the gamma-ray interaction properties of the alloys [32]. Vanaudenhove et al. used MC codes to study

Table 2 Comparison of the mass attenuation coefficients of composite shields with Bi and W fillers obtained using MCNPX, Geant4, and XCom data

Bi–W (as filler) and PDMS (as matrix) composite shield									
Energy (keV)	10% Bi–W			20% Bi–W			40% Bi–W		
	Diff [1]	Diff [2]	Diff [3]	Diff [1]	Diff [2]	Diff [3]	Diff [1]	Diff [2]	Diff [3]
20	24.19	0.56	23.76	15.43	1.88	13.81	8.18	0.73	8.85
40	3.87	0.22	3.65	3.95	0.15	4.10	2.03	0.31	1.72
60	4.13	0.73	3.42	10.31	1.05	11.48	9.37	1.11	8.35
80	19.40	0.40	19.08	7.92	0.84	7.14	29.18	0.62	28.73
100	4.38	0.34	4.05	2.97	0.29	3.27	12.61	0.10	12.52
120	12.56	0.55	12.08	14.71	0.19	14.93	17.67	0.68	17.11
140	17.18	0.40	16.85	14.00	0.86	14.99	28.50	0.51	28.14

Diff [1]: Difference in μ_m between MCNPX and XCom

Diff [2]: Difference in μ_m between Geant4 and XCom

Diff [3]: Difference in μ_m between MCNPX and Geant4

Table 3 Comparison of the mass attenuation coefficients of composite shields with Bi and Sn fillers obtained using MCNPX, Geant4, and XCom data

Bi–Sn (as filler) and PDMS (as matrix) composite shield									
Energy (keV)	10% Bi–Sn			20% Bi–Sn			40% Bi–Sn		
	Diff [1]	Diff [2]	Diff [3]	Diff [1]	Diff [2]	Diff [3]	Diff [1]	Diff [2]	Diff [3]
20	9.76	0.22	9.56	4.30	0.58	4.91	14.32	0.64	13.59
40	11.96	0.05	12.00	5.92	0.15	6.06	9.55	0.04	9.59
60	14.35	0.53	13.89	5.88	0.29	5.60	13.60	0.47	13.18
80	18.89	0.92	18.13	14.29	1.52	16.05	22.47	1.25	21.50
100	2.48	0.29	2.78	35.44	0.28	35.82	11.78	0.65	12.51
120	2.55	0.40	2.16	25.93	0.11	25.79	5.96	0.63	6.63
140	15.41	0.57	14.92	39.02	2.02	41.90	7.31	0.21	7.11

Diff [1]: Difference in μ_m between MCNPX and XCom

Diff [2]: Difference in μ_m between Geant4 and XCom

Diff [3]: Difference in μ_m between MCNPX and Geant4

Table 4 Comparison of the mass attenuation coefficients of composite shields with W and Sn fillers obtained using MCNPX, Geant4, and XCom data

W–Sn (as filler) and PDMS (as matrix) composite shield									
Energy (keV)	10% W–Sn			20% W–Sn			40% W–Sn		
	Diff [1]	Diff [2]	Diff [3]	Diff [1]	Diff [2]	Diff [3]	Diff [1]	Diff [2]	Diff [3]
20	7.77	0.43	7.37	1.98	0.13	2.11	2.11	0.16	2.27
40	10.96	0.01	10.97	7.35	0.01	7.35	12.16	0.03	12.19
60	8.87	0.78	8.16	2.94	1.04	1.92	19.59	0.74	18.99
80	2.62	0.65	3.29	10.78	0.00	10.78	7.25	0.13	7.13
100	1.24	0.67	1.92	9.52	0.13	9.66	10.50	0.60	9.96
120	7.64	0.00	7.64	4.55	0.20	4.76	22.59	0.00	22.59
140	6.97	0.66	7.67	6.06	1.15	4.85	26.80	0.35	26.54

Diff [1]: Difference in μ_m between MCNPX and XCom

Diff [2]: Difference in μ_m between Geant4 and XCom

Diff [3]: Difference in μ_m between MCNPX and Geant4

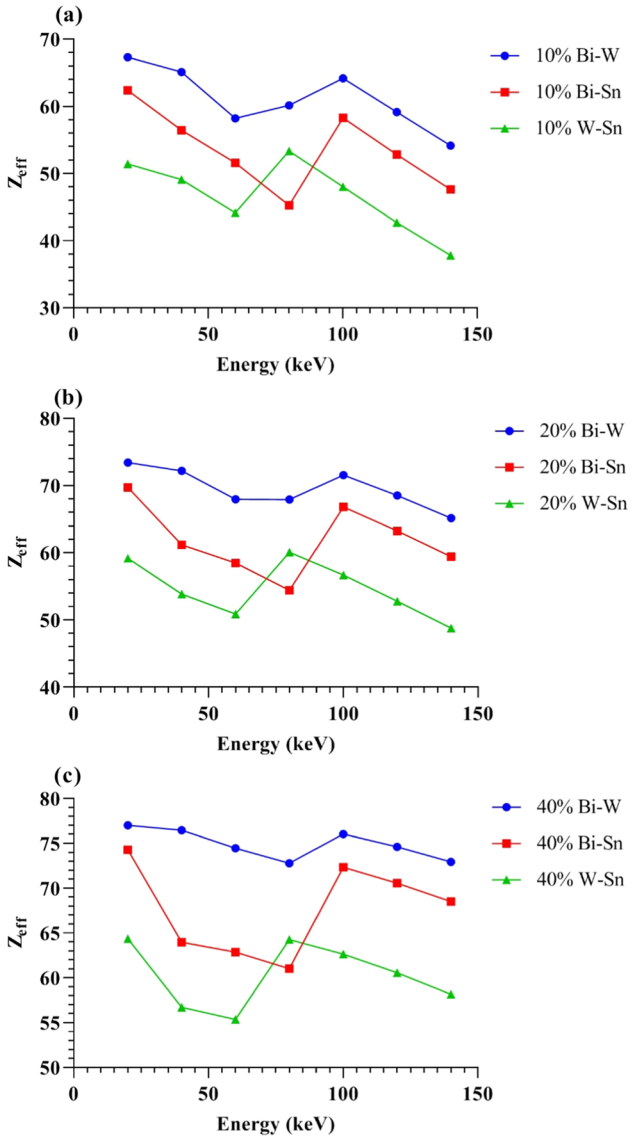

Fig. 6 Effective atomic number of multi-metal polymer composite shields with **a** 10%, **b** 20%, and **c** 40% fillers at 20–140 keV

the effectiveness of radiation shields in particle accelerator facilities, and reported that MCNPX and Geant4 are suitable for this purpose [33].

As indicated by Fig. 6, the values of Z_{eff} were maximum in the low-energy range (20–60 keV), minimum in the intermediate-energy range (60–80 keV), and moderate in the high-energy range (80–140 keV). The discontinuities in the intermediate-energy region were because of the K-edges of the constituent elements. Similar to μ_m, the decreasing trend with increasing energy was because of the *Z*-dependence of the cross sections for different photon interaction mechanisms, and was mainly photoelectric [32].

Z_{eff} for the Bi–W nanocomposite shields increased slightly as the energy increased from 60 to 100 keV. However, the Bi–Sn nanocomposite shields decreased as the energy increased from 60 to 80 keV, and then abruptly increased at 100 keV. The W–Sn nanocomposite shields increased as the energy increased to 80 keV and then decreased to the end of the energy range (140 keV). This behavioral difference was because of abrupt changes in the attenuation coefficient in the K-edge energy ranges. A comparison of these results with those of μ_m showed that the beam attenuation capacity of the shields increased with Z_{eff}. Sayyed and Elhouichet studied the rapid decrease in Z_{eff} with increasing incident photon energy (from 70 to 600 keV) for borotellurite (B_2O_3–TeO_2) glass samples [7]. High-atomic-number elements (Bi, W, and Sn) were used as fillers, and low-atomic-number elements (C, H, and Si) were applied as the main components of the PDSM matrix. The photoelectric absorption ability of the NPs was significantly higher than that of the PDSM. Thus, these particles play a key role in improving shielding performance (Fig. 2b).

The attenuation of MMPCs was higher than that of SMPCs because of the presence of elements with several high K-edges, which could absorb every part of the X-ray spectrum considered in this study. These types of MMPC radiation shields may be used to protect personnel and patients from several types of radiation, such as X-rays, gamma rays, and particles. This requires further theoretical and practical research.

5 Conclusion

In the present study, we designed and evaluated MMPCs with 10%, 20%, and 40% Bi, W, and Sn NPs, respectively, using MCNPX and Geant4 at photon energies between 20 and 140 keV.

The results indicate that the shielding performance of the Bi–W filler is better than that of the other single- and multi-metal nanocomposites at all concentrations and energies, probably because of the higher two K-edges and Z_{eff}, providing higher attenuation. In addition, the results obtained using both the Geant4 and MCNPX codes are in good agreement with the XCom theoretical data. However, Geant4 was more accurate in simulating the performance of radiation composites because of the manner in which the NPs were defined in this code.

Acknowledgements This study was financially supported by Isfahan University of Medical Sciences (MUI), Isfahan, Iran.

Author contributions NA: data acquisition by MCNPX, writing—original draft; RM: Simulation adviser, review and editing, original draft; SR: data acquisition using Geant4; SR: Methodology; PM and AS: Supervision, formal analysis, funding acquisition.

Data availability statement The datasets generated and analysed during the current study are available from the corresponding authors on reasonable request.

Declarations

Conflict of interest The authors declare no conflict of interest.

Ethical approval This study did not involve human participants.

References

1. United Nation. Sources and Effects of Ionizing Radiation Volume I. UNSCEAR 2000 Rep. 2000.
2. Mattsson S, Söderberg M. Radiation dose management in CT, SPECT/CT and PET/CT techniques. Radiat Prot Dosim. 2011;147:13–21. https://doi.org/10.1093/rpd/ncr261.
3. Alonso TC, Mourão AP, Santana PC, da Silva TA. Assessment of breast absorbed doses during thoracic computed tomography scan to evaluate the effectiveness of bismuth shielding. Appl Radiat Isot. 2016;117:55–7. https://doi.org/10.1016/j.apradiso.2016.03.018.
4. Parker MS, Kelleher NM, Hoots JA, Chung JK, Fatouros PP, Benedict SH. Absorbed radiation dose of the female breast during diagnostic multidetector chest CT and dose reduction with a tungsten-antimony composite breast shield: preliminary results. Clin Radiol. 2008;63:278–88.
5. Mansouri E, Mesbahi A, Malekzadeh R, Mansouri A. Shielding characteristics of nanocomposites for protection against X- and gamma rays in medical applications: effect of particle size, photon energy and nano-particle concentration. Radiat Environ Biophys. 2020;59:583–600. https://doi.org/10.1007/s00411-020-00865-8.
6. Mehnati P, Malekzadeh R, Sooteh MY. Application of personal non-lead nano-composite shields for radiation protection in diagnostic radiology: a systematic review and meta-analysis. Nanomed J. 2020;7:170–82.
7. Sayyed MI, Elhouichet H. Variation of energy absorption and exposure buildup factors with incident photon energy and penetration depth for boro-tellurite (B2O3-TeO2) glasses. Radiat Phys Chem. 2017;130:335–42.
8. Şakar E, Özpolat ÖF, Alım B, Sayyed MI, Kurudirek M. Phy-X / PSD: development of a user friendly online software for calculation of parameters relevant to radiation shielding and dosimetry. Radiat Phys Chem. 2020. https://doi.org/10.1016/j.radphyschem.2019.108496.
9. Tekin HO, Sayyed MI, Issa SAM. Gamma radiation shielding properties of the hematite-serpentine concrete blended with WO3 and Bi2O3 micro and nano particles using MCNPX code. Radiat Phys Chem. 2018;150:95–100.
10. Mansouri E, Mesbahi A, Malekzadeh R, Ghasemi Janghjoo A, Okutan M. A review on neutron shielding performance of nanocomposite materials. Int J Radiat Res. 2020;18:611–22.
11. Pelowitz DB. MCNPXTM User's Manual, Version 2.5.0. Los Alamos National Laboratory Report LA-CP-05-0369. 2005. https://www.scirp.org/%28S%28vtj3fa45qm1ean45vvffcz55%29%29/reference/ReferencesPapers.aspx?ReferenceID=1895609
12. Mendes M, Costa F, Figueira C, Madeira P, Teles P, Vaz P. Assessment of patient dose reduction by bismuth shielding in CT using measurements, GEANT4 and MCNPX simulations. Radiat Prot Dosim. 2015;165:175–81. https://doi.org/10.1093/rpd/ncv059.
13. Mahmoud ME, El-Khatib AM, Badawi MS, Rashad AR, El-Sharkawy RM, Thabet AA. Recycled high-density polyethylene plastics added with lead oxide nanoparticles as sustainable radiation shielding materials. J Clean Prod. 2018;176:276–87.
14. Mesbahi A, Mansouri E, Jangjoo AG, Tekin HO. Radiation protection characteristics of nano-concretes against photon and neutron beams. Smart Nanoconcretes Cem Mater Prop Model Appl. 2019. https://doi.org/10.1016/B978-0-12-817854-6.00019-2.
15. Verdipoor K, Alemi A, Mesbahi A. Photon mass attenuation coefficients of a silicon resin loaded with WO3, PbO, and Bi2O3 Micro and Nano-particles for radiation shielding. Radiat Phys Chem. 2018;147:85–90. https://doi.org/10.1016/j.radphyschem.2018.02.017.
16. Malekzadeh R, Mehnati P, Sooteh MY, Mesbahi A. Influence of the size of nano- and microparticles and photon energy on mass attenuation coefficients of bismuth–silicon shields in diagnostic radiology. Radiol Phys Technol. 2019;12:325–34. https://doi.org/10.1007/s12194-019-00529-3.
17. Nambiar S, Yeow JTW. Polymer-composite materials for radiation protection. ACS Appl Mater Interfaces. 2012;4:5717–26.
18. Mehnati P, Yousefi Sooteh M, Malekzadeh R, Divband B. Synthesis and characterization of nano Bi2O3 for radiology shield. Nanomed J. 2018;5:222–6.
19. Jamal AbuAlRoos N, Azman MN, Baharul Amin NA, Zainon R. Tungsten-based material as promising new lead-free gamma radiation shielding material in nuclear medicine. Phys Medica. 2020;78:48–57.
20. Gerward L, Guilbert N, Bjørn Jensen K, Levring H. X-ray absorption in matter. Reengineering XCOM. Radiat Phys Chem. 2001;60:23–4.
21. Zenobio MAF, Zenobio EG, da Silva TA, do Nogueira MS. Effective atomic numbers (Zeff) of based calcium phosphate biomaterials: a comparative study. Appl Radiat Isot. 2016;117:15–9.
22. Malekzadeh R, Sadeghi Zali V, Jahanbakhsh O, Okutan M, Mesbahi A. The preparation and characterization of silicon-based composites doped with BaSO4, WO3, and PbO nanoparticles for shielding applications in PET and nuclear medicine facilities. Nanomed J. 2020;7:324–34.
23. Agostinelli S, Allison J, Amako K, Apostolakis J, Araujo H, Arce P, et al. Geant4—a simulation toolkit. Nucl Instruments Methods Phys Res Sect A. 2003;506:250–303.
24. Berger MJ, Hubbell J. Engineering compendium on radiation shielding. Vienna: IAEA; 1968. p. 167–202.
25. Berger MJ, Hubbell JH, Seltzer SM, Chang J, Coursey JS, Sukumar R, et al. XCOM: photon cross sections database. NIST Stand Ref Database. 1998. https://www.nist.gov/pml/xcom-photon-cross-sections-database
26. Mesbahi A, Ghiasi H. Shielding properties of the ordinary concrete loaded with micro- and nano-particles against neutron and gamma radiations. Appl Radiat Isot. 2018;136:27–31.
27. El-Khatib AM, Abbas MI, Elzaher MA, Badawi MS, Alabsy MT, Alharshan GA, et al. Gamma attenuation coefficients of nano cadmium oxide/high density polyethylene composites. Sci Rep. 2019;9:16012. https://doi.org/10.1038/s41598-019-52220-7.
28. Mehnati P, Malekzadeh R, Yousefi SM. New bismuth composite shield for radiation protection of breast during coronary CT angiography. Iran J Radiol. 2019;16:e84763.
29. Sayyadi E, Mesbahi A, Zamiri RE, Nejad FS. A comprehensive Monte Carlo study to design a novel multi-nanoparticle loaded nanocomposites for augmentation of attenuation coefficient in the energy range of diagnostic X-rays. Pol J Med Phys Eng. 2021;27:279–89. https://doi.org/10.2478/pjmpe-2021-0033.
30. Mehnati P, Malekzadeh R, Sooteh MY. Use of bismuth shield for protection of superficial radiosensitive organs in patients undergoing computed tomography: a literature review and meta-analysis. Radiol Phys Technol. 2019;12:6–25.
31. Mehnati P, Malekzadeh R, Divband B, Yousefi SM. Assessment of the Effect of Nano-Composite Shield on Radiation Risk

Prevention to Breast During Computed Tomography. Iran J Radiol. 2020;17:e96002.
32. Singh VP, Medhat ME, Shirmardi SP. Comparative studies on shielding properties of some steel alloys using Geant4, MCNP, WinXCOM and experimental results. Radiat Phys Chem. 2015;106:255–60.
33. Vanaudenhove T, Dubus A, Pauly N, Stichelbaut F, De Smet V. Monte Carlo calculations with MCNPX and GEANT4 for general shielding study Application to a proton therapy center. Prog Nucl Sci Technol. 2014;4:422–6.